PCCP

PAPER

Cite this: *Phys. Chem. Chem. Phys.*, 2025, **27**, 19703

# The impact of electronic correlations on the structural stability and spectral properties of ferrocene and polyferrocene under pressure

Alexey A. Dyachenko, *[ab] Alexey V. Lukoyanov, [abc] Vladimir I. Anisimov [abc] and Artem R. Oganov [b]

Received 4th April 2025, Accepted 11th August 2025

DOI: 10.1039/d5cp01302j

rsc.li/pccp

In this work, the electronic, spectral, and structural properties of ferrocene and polyferrocene under pressure have been investigated using DFT and DFT+DMFT methods taking into account dynamic electronic correlations. It is found that polyferrocene crystalizes in three different phases with transitions at 80 and 200 GPa. The calculated DFT+DMFT enthalpy of ferrocene and polyferrocene indicates a possibility of ferrocene transitioning into a polymerized phase at about 80 GPa. It is demonstrated that polyferrocene undergoes an insulator-to-metal transition under pressure, closing a gap of 2.45 eV. However, while the insulating state of polyferrocene can be described as a band insulator, the insulator-to-metal transition is found to be caused by a structural transition into a metallic high-pressure phase of polyferrocene which is defined by strongly correlated behavior of Fe ions.

## 1. Introduction

Since its discovery, ferrocene $Fe(C_5H_5)_2$ fascinated researchers as one of the most unique organometallic compounds due to its electronic and structural properties. Ferrocene was obtained accidentally as a byproduct of the synthesis of dihydrofulvalene in 1951,[1,2] and its structure was determined by reactivity analysis[3] and was confirmed by crystallographic studies later.[4,5] After its discovery more than half a century ago, ferrocene, along with other metallocenes and their derivatives, became one of the main directions of organometallic chemistry and found many applications in many fields, such as catalysis, redox, medicine, aerospace materials, medicine, electroanalytical sensing, energy storage, memory devices, *etc.*[6–13] Ferrocene at room temperature consists of an iron center with the oxidation state +2 located between two cyclopentadienyl (Cp) rings with a negative charge each. The six electrons from the iron ion pair with six electrons from each Cp ring to form an 18-electron configuration.[14] Following the 18-electron rule, ferrocene is a very stable, mild redox complex with predictable and reversible oxidation properties. Additionally, ferrocene exhibits a high electron transfer rate due to the stability of ferrocenium $Fe(C_5H_5)_2^+$ cations, which can easily be formed as the one-electron oxidation potential *versus* saturated calomel electrode is around 0.4 V.[15] Due to such properties, the ferrocenium/ferrocene redox pair serves as a reference system for determining the redox potential of different systems.[16]

Apart from the gas phase, in which the Cp rings are in eclipsed ($D_{5h}$) conformation,[17] ferrocene is known to conform in four different phases: a phase with monoclinic space group $P2_1/n$,[4] which is stable under ambient conditions, for which the Cp rings are staggered ($D_{5d}$), and then at 3.24 GPa, it transforms into a phase with ordered Cp rings.[18,19] At low temperature, ferrocene transforms into eclipsed phases: to a triclinic phase at 164 K with almost fully eclipsed Cp rings[20] and to an orthorhombic phase at 98 K with fully eclipsed rings.[21] The noteworthy properties of ferrocene, which contribute to the stability of the compound, are the low Cp ring rotation barrier[22] and the low energy required for a reversible one-electron oxidation.[23]

Density functional theory (DFT) is a standard *ab initio* method for investigating the properties of materials.[24] Several works reveal that DFT is successful in describing the structural, electronic, magnetic, optical, redox, and other properties of metallocenes and related compounds.[25,26] An *ab initio* study using the evolutionary structure prediction algorithm USPEX[27] with DFT suggested that at and above 220 GPa, ferrocene forms metallic polymeric chains.[28] In this work, we employ density functional theory enhanced by the dynamical mean-field theory (DFT+DMFT)[29–32] to investigate the effects of pressure and dynamic electronic correlations on the formation of ferrocene polymer chains.

[a] *M. N. Mikheev Institute of Metal Physics of Ural Branch of Russian Academy of Sciences, Yekaterinburg 620108, Russia. E-mail: dyachenko@imp.uran.ru*
[b] *Skolkovo Institute of Science and Technology, Moscow 121205, Russia*
[c] *Institute of Physics and Technology, Ural Federal University, Yekaterinburg 620002, Russia*

## 2. Methods

The computational scheme of the DFT+DMFT method[29–32] employed in this work starts with the self-consistent DFT calculations. The generalized gradient approximation[33] implemented in the Quantum ESPRESSO package[34] was used with dispersion correction to produce a noninteracting Hamiltonian and then set up a many-body Hamiltonian. Then the DMFT equations for this Hamiltonian were solved self-consistently. For the Fe-3d, 3p, 3s, C-2s, 2p, and H-1s orbitals, we constructed a basis set of Wannier functions[35,36] employing the projection procedure described in detail in ref. 37. All bands of the basis set formed by the chosen states were included and projected on the Bloch functions for these bands.

The interaction matrix for the quantum impurity model was parameterized by the values of the Coulomb repulsion parameter $U$ and Hund exchange parameter $J_H$ in the density–density approximation. The interaction parameters were calculated using the self-consistent constrained DFT approach[38–40]; the Fe-3d Coulomb repulsion parameter is $U = 7.1$ eV, and the Hund parameter is $J_H = 0.9$ eV.

The continuous-time quantum Monte Carlo hybridization-expansion solver from the AMULET[41] package was employed to solve the effective DMFT quantum impurity problem.[42] Some code from the ALPS Project was used for the calculations.[43] The ELK[44] code was used for charge self-consistent DMFT calculations as implemented within the AMULET package. The presented spectral functions were calculated from real frequency lattice Green's functions $G(\omega)$ using the Pade approximants[45] for the analytical continuation to the real energy axis, as implemented in the AMULET package. The DMFT calculations were performed at an electronic temperature of $T = 1000$ K for computational efficiency, while several calculations at various volumes were performed at an electronic temperature of $T = 300$ K to ensure that no significant changes in the magnetic, electronic, or spectral properties occur at higher $T$.

The available published crystal structure data for polyferrocene reported by Gain *et al.*,[28] which are used in this work, were obtained with the evolutionary USPEX algorithm in VASP using PBE functionals including corrections for van der Waals forces in the form of Grimme's DFT-D2 corrections. To remain consistent with the published results, for the ferrocene structures, we employed PBE functionals and included Grimme's DFT-D2 corrections. To obtain the crystal structure of ferrocene under pressure, we performed variable-cell relaxations with constrained pressure parameters as implemented in Quantum ESPRESSO.

The total energies from DFT and DFT+DMFT were fit using the Rose–Vinet equation of state[46]:

$$E(V) = E_0 + \frac{2B_0V_0}{(B_0'-1)^2}\left\{2 - \left[5 + 3\left(\frac{V}{V_0}\right)^{\frac{1}{3}}(B_0' - 1 - 3B_0')\right] \times \exp\left[-\frac{3}{2}(B_0'-1)\left[\left(\frac{V}{V_0}\right)^{\frac{1}{3}} - 1\right]\right]\right\} \quad (1)$$

For systems with complex phase behavior, it is necessary to fit multiple equations of state at once to detect phase transitions. To this end, we combine several equations of state using some step function, Gauss error function erf in this case. Then the final equation to fit was

$$E_{\text{combined}}(V) = \frac{1}{2}\left\{\left[1 + \text{erf}\left(\frac{V-p}{w}\right)\right]E_1(V) + \left[1 - \text{erf}\left(\frac{V-p}{w}\right)E_2(V)\right]\right\}, \quad (2)$$

where both $E_1$ and $E_2$ had four of their own vaiables to fit ($E_0$, $V_0$, $B_0$, and $B_0'$). Additionally, parameters $p$ and $w$, which act as the position and width of the step function, were also unconstrained and the variables of the minimization problem. In practice, we are limited not only by the number of calculated volume points but also by a stochastic noise from the DMFT algorithm. Thus, for the stability of the algorithm, we used two equations of state in the minimization problem, solving them for data of different volume ranges to find and fit all present phases correctly.

## 3. Results

Our DFT+DMFT calculations were performed for ferrocene and polyferrocene structures under pressure. For the polyferrocene, we used published structures by Gain *et al.*,[28] which were predicted using the evolutionary structure prediction algorithm USPEX along with density functional theory calculations. The polyferrocene structures were used as is, and no further modifications were made by the authors. For the ferrocene under pressure, we started with the published experimental structure[47] and performed structural optimizations as explained in Section 2.

### 3.1. Spectral properties

First, we examine the spectral properties of poly-Fc and Fc as predicted by DFT+DMFT calculations. The DFT+DMFT spectral functions $A(w)$ of poly-Fc C-p and Fe-d states are presented in Fig. 1. Both C-p and Fe-d spectral functions become metallic, and an insulator-to-metal transition is observed under pressure in poly-Fc at about 140 Å$^3$. Ferrocene, on the other hand, remains insulating at all considered volumes. The calculated DFT+DMFT spectral gap of poly-Fc is presented in Fig. 2. At ambient pressure, the calculated gap is 2.0 eV, increases to about 2.55 eV at 170 Å$^3$, and afterward drops to 2.45 eV at 140 Å$^3$. At a volume of 136 Å$^3$ and lower, the spectral gap closes and the poly-Fc becomes metallic. Here, mainly due to effects of temperature, we define the gap as a distance between Fe-d band edges. Furthermore, Pade approximants of local Green's functions of the uncorrelated states that are far from the Fermi energy retain their integral properties and reproduce imaginary part of Green's functions, but usually lack some fine details on the real axis. It is a known shortcoming of an analytic continuation. In particular, it may appear that C-p states are wide and encroach on the Fermi level at ambient pressure, far closer

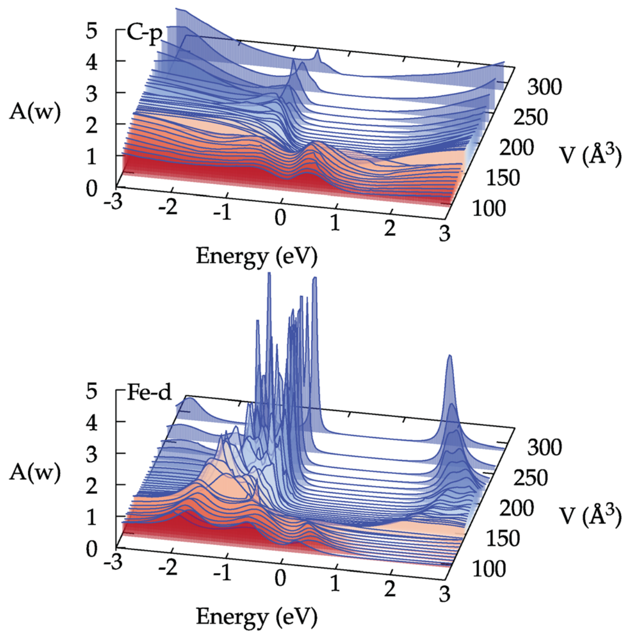


Fig. 1 Spectral functions $A(w)$ of C-p and Fe-d in poly-Fc under pressure obtained *via* DFT+DMFT calculations. The Fermi energy is zero.

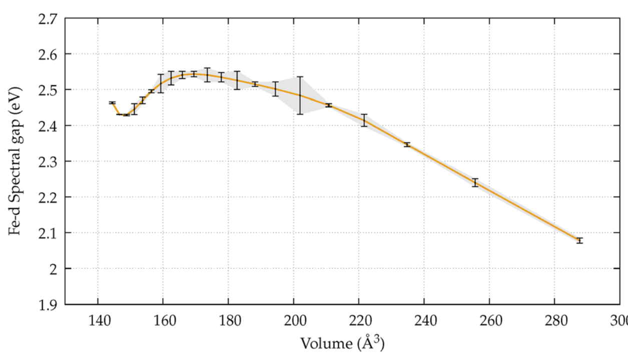


Fig. 2 Spectral gap of poly-Fc under pressure calculated from DFT+DMFT Fe-d spectral functions $A(w)$.

than Fe-d states. In the momentum-dependent spectral functions $A(k,w)$ which are calculated using self-energy instead, C-p states appear to be more defined: they are centered at about 4.4 eV and range from 3.5 to 5.1 eV. The spectral functions of the correlated Fe-d states obtained from local Green's functions are accurate. In contrast to DFT+DMFT, the DFT calculations predict the gap to be about 2.62–2.5 eV up to 165 Å$^3$, then at lower volumes, the gap decreases and an insulator-to-metal transition occurs at about 140 Å$^3$.[28] Optical and spectroscopic measurements report that a HOMO–LUMO gap in ferrocene is about 2.73–2.93 eV at ambient pressure.[48,49]

The DFT+DMFT results show a strong density renormalization due to the dynamic electronic effects that we account for in DMFT. In Fig. 3, we present the DFT+DMFT momentum-dependent spectral function $A(k,w)$ and the DFT+U band structure for 136 Å$^3$ when poly-Fc becomes metallic. At ambient pressure, poly-Fc can be characterized as a non-magnetic uncorrelated band insulator; the DFT+DMFT calculations at volumes down to 136 Å$^3$ point to a lack of dynamic correlations in poly-Fc. The DFT results indicate the occurrence of transition from the band insulator to the metal at 136 Å$^3$. Furthermore, the DFT+U calculations result in an insulating band structure at all considered volumes, indicating that accounting for Coulomb interactions in a static form within the DFT+U method is not sufficient to correctly describe the electronic structure of poly-Fc under pressure. On the other hand, the obtained DFT+DMFT momentum-resolved spectral functions show not only a metallic state but also a strong density renormalization with significant changes in the electronic structure, which is indicative of strong electronic correlations.

### 3.2. Phase transitions

Next, we analyze the structural stability and bulk properties of poly-Fc and ferrocene. The observed behavior of spectral properties under pressure in poly-Fc is quite complex, so that a single equation of state could be insufficient for a proper description of poly-Fc behavior. We employed a method of fitting multiple equations of state at the same time with a blending function in-between from a whole set of data points. The calculated DFT+DMFT free energy and the resulting fits are presented in Fig. 4. As a result, from the DFT+DMFT free energies, we were able to distinguish three different phases of poly-Fc under pressure; these will be designated as poly-Fc I from 394 to 200 Å$^3$, poly-Fc II from 200 to 144 Å$^3$, and poly-Fc III from 136 Å$^3$ and lower. These poly-Fc phase distinctions are consistent with the dynamics of the optical gap we have shown. It is important to note that the calculated total energies of Fc indicate no significant effect from accounting for Coulomb correlations.

The parameters for the Rose–Vinet equation of state are presented in Table 1. Within DFT, which lacks strong electronic correlations, the parameters for poly-Fc are misleadingly similar to those of ferrocene. Our DFT and DFT+DMFT calculations for ferrocene, due to its uncorrelated electronic structure, resulted in the same values of parameters, albeit for a static shift in the total energy of about 4.5 eV due to Coulomb corrections.

With the resulting parameters of the equations of state, we calculate the volume *versus* pressure dependence of poly-Fc, as presented in Fig. 5a. We observe a small volume collapse of about 5% between poly-Fc I and poly-Fc II phases. The calculated DFT+DMFT enthalpies of poly-Fc and ferrocene (see Fig. 5b) show that ferrocene can transition into the poly-Fc II phase at about 80 GPa, skipping the poly-Fc I phase. Only at 290 GPa, the poly-Fc III phase overtakes the ferrocene structure. It is interesting to note that, according to our calculations, the poly-Fc II phase remains more energetically favorable than the ferrocene structure or the poly-Fc III phase at higher pressures. According to the DFT calculations, which were the basis for structure relaxation, poly-Fc II and poly-Fc III follow the same equation of state, and the transition occurs between 219 and 257 GPa. However, when accounting for strong electronic and dynamic correlations in poly-Fc III, the transition pressure

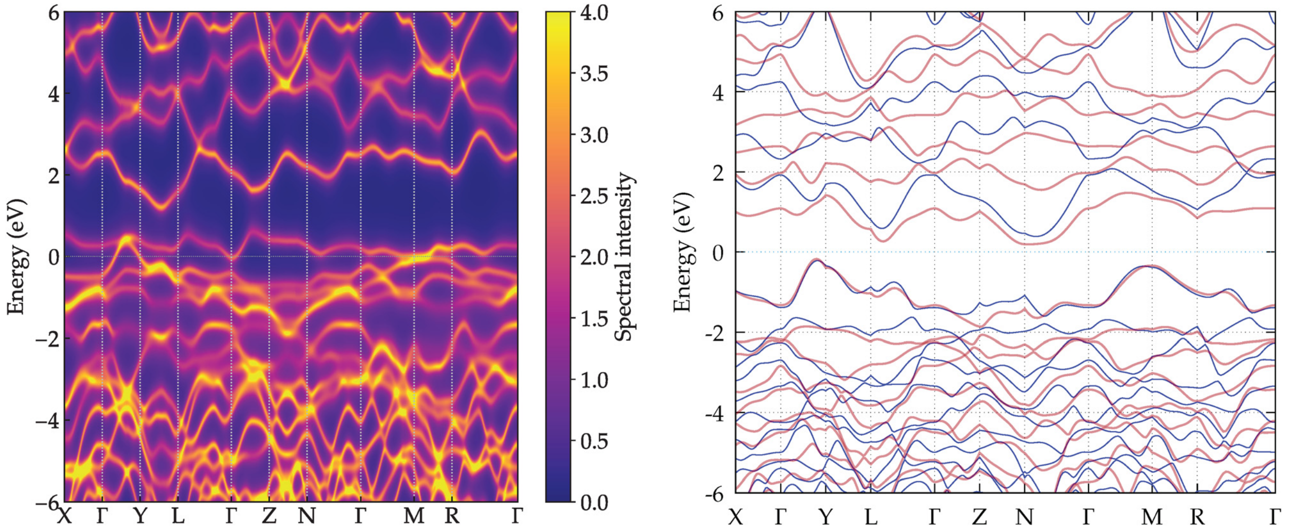


(a) (b)

Fig. 3 DFT+DMFT momentum-dependent spectral functions $A(k,w)$ (a) and DFT+U band structures of poly-Fc (b) at 136 Å$^3$. The Fermi energy is set to zero.

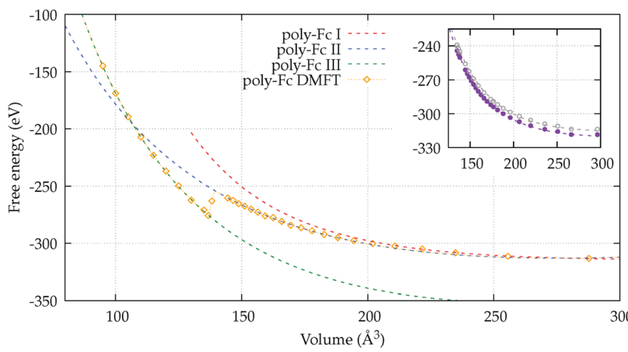


Fig. 4 DFT and DFT+DMFT free energy of poly-Fc under pressure. The dashed lines represent each separate component of the Rose–Vinet fit of an equation of state and correspond to each phase of poly-Fc, respectively. Symbols show the free energy obtained from the calculations. Inset: DFT and DFT+DMFT free energy of Fc under pressure.

Table 1 Parameters of Rose–Vinet equations of state of ferrocene and poly-Fc obtained by DFT and DFT+DMFT

| Phase | $E_0$ (eV) | $V_0$ (Å$^3$) | $B_0$ (GPa) | $B'_0$ |
|---|---|---|---|---|
| poly-Fc-I | −314.638 | 351.975 | 16.4063 | 7.8961 |
| poly-Fc-II | −313.099 | 275.445 | 134.84 | 2.53602 |
| poly-Fc-III | −353.047 | 276.3 | 127.897 | 3.69985 |
| poly-Fc (DFT) | −319.039 | 346.693 | 20.8265 | 6.39281 |
| Fc (DFT) | −320.391 | 346.164 | 20.2524 | 6.72189 |
| Fc | −315.618 | 347.672 | 19.9725 | 6.73963 |

range is much wider: between 180 and 290 GPa. The predicted phase transition pressure indicates that poly-Fc would be almost incompressible at a pressure of 110 GPa. Within DFT, these poly-Fc structures have the lowest energy at a corresponding volume, but once we take into account strong electronic correlations and dynamic effects, it appears that the structures are no longer favorable, and thus the anomaly in poly-Fc II to poly-Fc III transition is observed.

### 3.3. Electronic structure

Our calculations show that the poly-Fc III phase exhibits the most peculiar properties. Only at 136 Å$^3$ (about 300 GPa), in the phase poly-Fc III, poly-Fc forms two additional C–C bonds between neighboring Cp rings. The formation of two extra C–C bonds is a structural effect due to the distortion of the cyclopentadienyl rings. We have calculated electron localization function (ELF) for poly-Fc at 136 Å$^3$ (see Fig. 6). The ELF for poly-Fc demonstrates strong electron localization at the bonds between the closest carbon atoms of the neighboring Cp rings, similar to localization between the carbon atoms in the ring. At this volume, the Cp ring has bond lengths of 1.37, 1.40, and 1.44 Å, and the distance between the closest C atoms of the two rings is 1.45 Å. At the same time, even the extreme compression of ferrocene (down to 75 Å$^3$) shows no such localization outside of ferrocene molecules. Evidently, the formation of the two C–C bonds has a crucial effect on the electronic structure of poly-Fc III.

We have conducted DFT+DMFT calculations for the poly-Fc III structure at higher volumes of 395, 333, 272, 211, and 150 Å$^3$. The obtained poly-Fc III spectral functions of C-p and Fe-d are presented in Fig. 7. In contrast to poly-Fc I and II, the spectral functions of the poly-Fc III structure are metallic at all pressures due to the C-p density. Furthermore, the Fe-d ion undergoes a Mott-like transition. To show that, we present the calculated electronic configurations of the Fe-d quantum impurity of poly-Fc in Fig. 8. At ambient pressure, the Fe-d quantum impurity of poly-Fc I has an occupancy

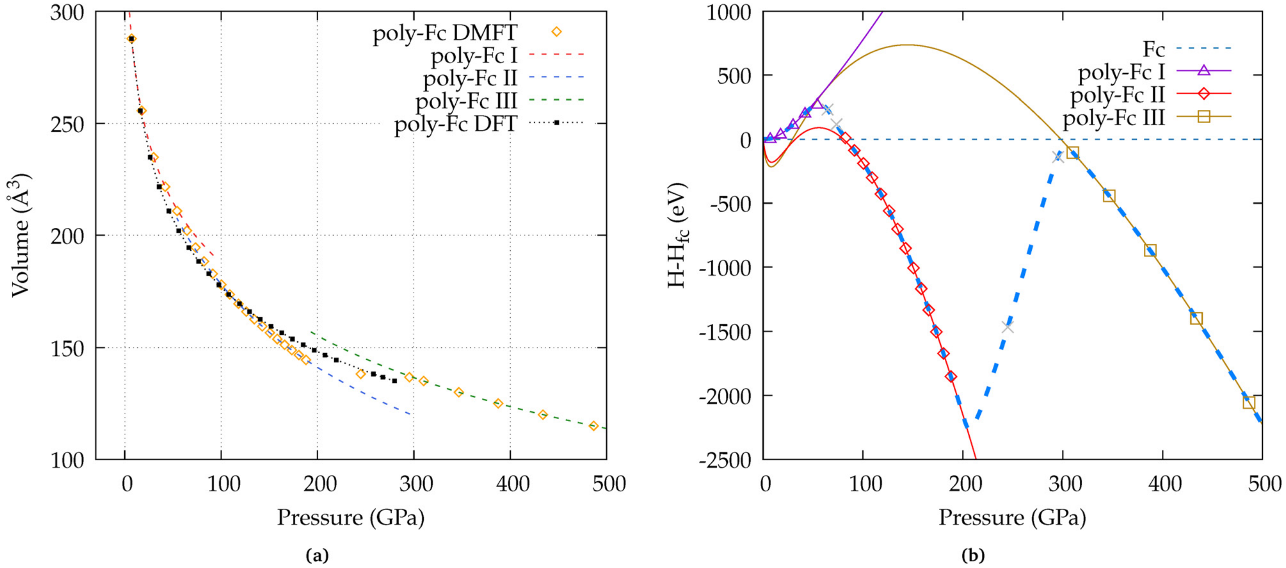


Fig. 5 (a) DFT and DFT+DMFT equations of state of poly-Fc under pressure. The dashed lines represent each phase corresponding to the Rose–Vinet fit of an equation of state. (b) DFT+DMFT enthalpy of poly-Fc with respect to the enthalpy of Fc (dashed reference line at zero). The solid lines represent each phase corresponding to the fit of an equation of state. The thick dashed line represents the total combined poly-Fc enthalpy. The cross symbols are the data points we excluded from the equation of state minimization problem.

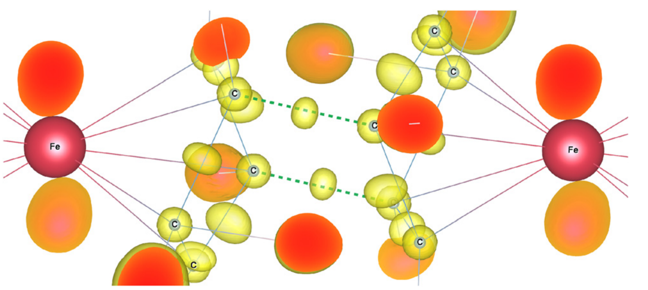


Fig. 6 Electron localization function of poly-Fc III at 136 Å$^3$. The two extra bonds between cyclopentadienyl rings are marked with dashed lines.

of $n_{\text{Fe-d}} = 6.8$ electrons, as a combination of $N = 6$, 7, and 8 low-spin states, corresponding to the $d^6$ configuration of the Fe ion, with a local magnetic moment of $\sqrt{\langle \mu_z^2 \rangle} = 1.44\mu_B$. On the other hand, at ambient pressure, the Fe-d quantum impurity of the poly-Fc III structure is in the $d^6$ configuration and has an occupancy of $n_{\text{Fe-d}} = 6.16$ electrons, which consists of high-spin $N = 6$ and 7 states and has a local magnetic moment of $\sqrt{\langle \mu_z^2 \rangle} = 3.69\mu_B$. Poly-Fc III undergoes a spin transition when compressed to volumes between 200 and 150 Å$^3$ (60 and 150 GPa, respectively). At 136 Å$^3$, the value of the Fe-d local magnetic moment $\sqrt{\langle \mu_z^2 \rangle}$ in poly-Fc III is $1.69\mu_B$, with the Fe-d quantum impurity exhibiting a mix of low and intermediate spin states and an occupancy of $n_{\text{Fe-d}} = 6.97$.

At first glance, the arrangement of bonds between the Cp rings resembles a mixed-valence complex biferrocenium, where two ferrocene molecules are connected by one extra C–C bond, resulting in one of the iron ions being in the $d^5$ configuration.[50] In our calculations, we observe a decreased occupancy at ambient pressure: 6.16 electrons in poly-Fc III *versus* 6.8 electrons in poly-Fc I; however, the Fe ion remains in the $d^6$ configuration.

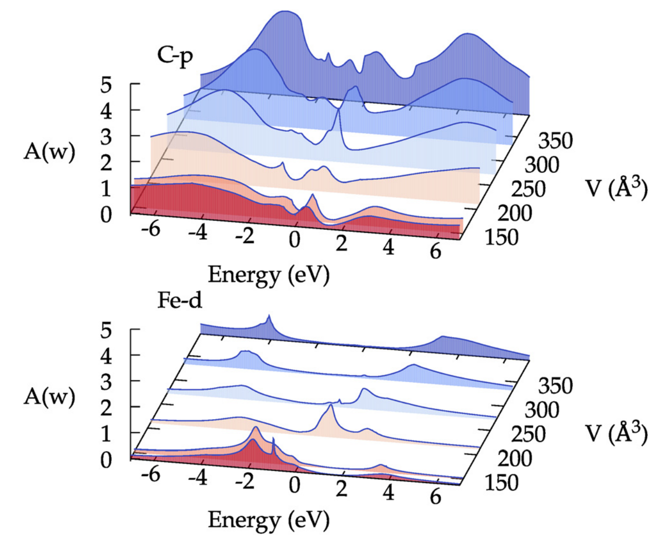


Fig. 7 Spectral functions of the poly-Fc III phase under pressure: (top) C-p and (bottom) Fe-d spectral functions. The Fermi energy is set to zero.

## 4. Conclusions

We employed the DFT+DMFT method to investigate the electronic structure and structural stability of ferrocene and polyferrocene under pressure. We calculated the equations of state and found three distinct phases in polyferrocene: poly-Fc I from

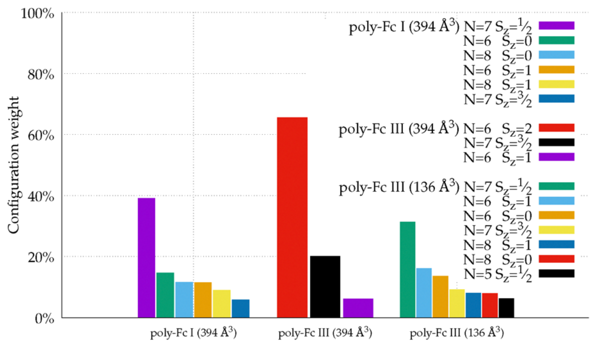


Fig. 8 Weights of Fe-d quantum impurity electronic configurations within DMFT.

AP to 80 GPa, poly-Fc II up to 200 GPa, and poly-Fc III at higher pressures. At 80 GPa, we found that ferrocene can undergo a structural transition into polyferrocene. We found that the insulator-to-metal transition in polyferrocene under pressure is caused by a structural transition from insulating poly-Fc I and poly-Fc II phases, with spectral gaps of 2.0 and 2.55 eV, respectively, to a strongly correlated poly-Fc III phase which is metallic at all pressures. Our findings indicate that polyferrocene is a system where electronic correlations are in extrema: at lower pressures, the structure experiences almost no correlations and can be quite adequately described by DFT. On the other hand, under high pressure, the effects of strong electronic correlations are so important that it is crucial to take them into account during structural optimization for the correct evaluation of phase transitions. The calculated enthalpy shows, that, due to strong electronic correlations in the polymerized poly-Fc III phase, poly-Fc II still remains more favorable under high pressure.

## Author contributions

Conceptualization: A. R. O. and V. I. A.; methodology: A. A. D. and A. V. L.; software: A. A. D.; validation: A. V. L., V. I. A. and A. R. O.; formal analysis: A. A. D. and A. V. L.; investigation: A. A. D. and A. V. L.; resources: A. R. O. and A. V. L.; data curation: A. A. D. and A. V. L.; writing – original draft preparation: A. A. D. and A. V. L.; writing – review and editing: A. A. D., A. V. L., and A. R. O.; visualization: A. A. D.; supervision: A. R. O., V. I. A., and A. V. L.; project administration: A. R. O. and V. I. A.; funding acquisition: A. R. O. All authors have read and agreed to the published version of the manuscript.

## Conflicts of interest

The authors declare no conflicts of interest. The funders had no role in the design of the study, in the collection, analyses, or interpretation of data, in the writing of the manuscript, or in the decision to publish the results.

## Data availability

The code for the AMULET package can be found at **https://amulet-code.org**. This study was carried out using publicly available crystal structure data from P. Gain, R. Jana and A. Datta, *The Journal of Physical Chemistry A*, 2021, **125**, 3362–3368, DOI: **https://doi.org/10.1021/acs.jpca.1c01205**

## Acknowledgements

The results of Sections 3.1 and 3.2 (spectral properties and phase transitions) were obtained with support from the grant of the Russian Science Foundation (project 19-72-30043-P). The results of Section 3.3 (electronic structure) were obtained within the framework of the state assignment of the Ministry of Science and Higher Education of the Russian Federation for IMP UrB RAS. The authors are thankful to Dr Pranab Gain for the data provided from ref. 28.

## Notes and references

1 T. J. Kealy and P. L. Pauson, *Nature*, 1951, **168**, 1039–1040.
2 S. A. Miller, J. A. Tebboth and J. F. Tremaine, *J. Chem. Soc.*, 1952, 632.
3 G. Wilkinson, M. Rosenblum, M. C. Whiting and R. B. Woodward, *J. Am. Chem. Soc.*, 1952, **74**, 2125–2126.
4 P. F. Eiland and R. Pepinsky, *J. Am. Chem. Soc.*, 1952, **74**, 4971.
5 J. D. Dunitz, L. E. Orgel and A. Rich, *Acta Crystallogr.*, 1956, **9**, 373–375.
6 D. Astruc, *Eur. J. Inorg. Chem.*, 2017, 6–29.
7 L. Cunningham, A. Benson and P. J. Guiry, *Org. Biomol. Chem.*, 2020, **18**, 9329–9370.
8 L. Fabbrizzi, *ChemTexts*, 2020, **6**, 22.
9 G. Sruthi, K. Shakeela, R. Shanmugam and G. Ranga Rao, *Phys. Chem. Chem. Phys.*, 2020, **22**, 3329–3344.
10 Z. Huang, H. Yu, L. Wang, X. Liu, T. Lin, F. Haq, S. Z. Vatsadze and D. A. Lemenovskiy, *Coord. Chem. Rev.*, 2021, **430**, 213737.
11 M. Zhang, F. Zhao, H. Li, S. Dong, Y. Yang, X. Hou, T. An and Z. Jiang, *Phys. Chem. Chem. Phys.*, 2021, **23**, 17567–17575.
12 U. Rauf, G. Shabir, S. Bukhari, F. Albericio and A. Saeed, *Molecules*, 2023, **28**, 5765.
13 H. Ren and H. Gu, *Phys. Chem. Chem. Phys.*, 2025, **27**, 4950–4958.
14 G. Wilkinson, *J. Organomet. Chem.*, 1975, **100**, 273–278.
15 N. G. Connelly and W. E. Geiger, *Chem. Rev.*, 1996, **96**, 877–910.
16 G. Gritzner and J. Kuta, *Pure Appl. Chem.*, 1984, **56**, 461–466.
17 R. K. Bohn and A. Haaland, *J. Organomet. Chem.*, 1966, **5**, 470–476.
18 D. Paliwoda, K. Kowalska, M. Hanfland and A. Katrusiak, *J. Phys. Chem. Lett.*, 2013, **4**, 4032–4037.
19 D. Paliwoda, M. Hanfland and A. Katrusiak, *J. Phys. Chem. C*, 2019, **123**, 25719–25723.

20 P. Seiler and J. D. Dunitz, *Acta Crystallogr., Sect. B*, 1979, **35**, 2020–2032.

21 P. Seiler and J. D. Dunitz, *Acta Crystallogr., Sect. B*, 1982, **38**, 1741–1745.

22 A. Haaland and J.-E. Nilsson, *Chem. Commun.*, 1968, 88–89.

23 R. R. Gagne, C. A. Koval and G. C. Lisensky, *Inorg. Chem.*, 1980, **19**, 2854–2855.

24 W. Kohn and L. J. Sham, *Phys. Rev.*, 1965, **140**, A1133–A1138.

25 M. Bühl and H. Kabrede, *J. Chem. Theory Comput.*, 2006, **2**, 1282–1290.

26 T. P. Gryaznova, S. A. Katsyuba, V. A. Milyukov and O. G. Sinyashin, *J. Organomet. Chem.*, 2010, **695**, 2586–2595.

27 A. R. Oganov and C. W. Glass, *J. Chem. Phys.*, 2006, **124**, 244704.

28 P. Gain, R. Jana and A. Datta, *J. Phys. Chem. A*, 2021, **125**, 3362–3368.

29 A. Georges, G. Kotliar, W. Krauth and M. J. Rozenberg, *Rev. Mod. Phys.*, 1996, **68**, 13–125.

30 K. Held, A. K. McMahan and R. T. Scalettar, *Phys. Rev. Lett.*, 2001, **87**, 276404.

31 K. Held, I. A. Nekrasov, G. Keller, V. Eyert, N. Blümer, A. K. McMahan, R. T. Scalettar, T. Pruschke, V. I. Anisimov and D. Vollhardt, *Phys. Status Solidi B*, 2006, **243**, 2599–2631.

32 G. Kotliar, S. Y. Savrasov, K. Haule, V. S. Oudovenko, O. Parcollet and C. A. Marianetti, *Rev. Mod. Phys.*, 2006, **78**, 865–951.

33 J. P. Perdew, K. Burke and M. Ernzerhof, *Phys. Rev. Lett.*, 1996, **77**, 3865–3868.

34 P. Giannozzi, S. Baroni, N. Bonini, M. Calandra, R. Car, C. Cavazzoni, D. Ceresoli, G. L. Chiarotti, M. Cococcioni, I. Dabo, A. D. Corso, S. de Gironcoli, S. Fabris, G. Fratesi, R. Gebauer, U. Gerstmann, C. Gougoussis, A. Kokalj, M. Lazzeri, L. Martin-Samos, N. Marzari, F. Mauri, R. Mazzarello, S. Paolini, A. Pasquarello, L. Paulatto, C. Sbraccia, S. Scandolo, G. Sclauzero, A. P. Seitsonen, A. Smogunov, P. Umari and R. M. Wentzcovitch, *J. Phys.: Condens. Matter*, 2009, **21**, 395502.

35 G. H. Wannier, *Phys. Rev.*, 1937, **52**, 191–197.

36 N. Marzari and D. Vanderbilt, *Phys. Rev. B: Condens. Matter Mater. Phys.*, 1997, **56**, 12847–12865.

37 D. Korotin, A. V. Kozhevnikov, S. L. Skornyakov, I. Leonov, N. Binggeli, V. I. Anisimov and G. Trimarchi, *Eur. Phys. J. B*, 2008, **65**, 91–98.

38 M. Cococcioni and S. de Gironcoli, *Phys. Rev. B: Condens. Matter Mater. Phys.*, 2005, **71**, 035105.

39 H. Hsu, K. Umemoto, M. Cococcioni and R. Wentzcovitch, *Phys. Rev. B: Condens. Matter Mater. Phys.*, 2009, **79**, 125124.

40 I. Timrov, N. Marzari and M. Cococcioni, *Comput. Phys. Commun.*, 2022, **279**, 108455.

41 https://www.amulet-code.org (accessed on 31 March 2025).

42 P. Werner and A. J. Millis, *Phys. Rev. B: Condens. Matter Mater. Phys.*, 2006, **74**, 155107.

43 A. Albuquerque, F. Alet, P. Corboz, P. Dayal, A. Feiguin, S. Fuchs, L. Gamper, E. Gull, S. Gürtler, A. Honecker, R. Igarashi, M. Körner, A. Kozhevnikov, A. Läuchli, S. Manmana, M. Matsumoto, I. McCulloch, F. Michel, R. Noack, G. Pawłowski, L. Pollet, T. Pruschke, U. Schollwöck, S. Todo, S. Trebst, M. Troyer, P. Werner and S. Wessel, *J. Magn. Magn. Mater.*, 2007, **310**, 1187–1193.

44 https://elk.sourceforge.net/ (accessed on 31 March 2025).

45 K. S. D. Beach, R. J. Gooding and F. Marsiglio, *Phys. Rev. B: Condens. Matter Mater. Phys.*, 2000, **61**, 5147–5157.

46 P. Vinet, J. R. Smith, J. Ferrante and J. H. Rose, *Phys. Rev. B: Condens. Matter Mater. Phys.*, 1987, **35**, 1945–1953.

47 C. P. Brock and Y. Fu, *Acta Crystallogr., Sect. B*, 1997, **53**, 928–938.

48 P. A. Dowben, D. C. Driscoll, R. S. Tate and N. M. Boag, *Organometallics*, 1988, **7**, 305–308.

49 K. M. Lancaster, K. D. Finkelstein and S. DeBeer, *Inorg. Chem.*, 2011, **50**, 6767–6774.

50 D. O. Cowan, C. LeVanda, J. Park and F. Kaufman, *Acc. Chem. Res.*, 1973, **6**, 1–7.